Comparative Medicine
Copyright 2020
by the American Association for Laboratory Animal Science

Vol 70, No 3
June 2020
Pages 216–232

Original Research

Effects of Colonization of Gnotobiotic Swiss Webster Mice with *Helicobacter bilis*

Mark T Whary,[1,*,‡] Chuanwu Wang,[1,‡] Catherine F Ruff,[1] Mallory J DiVincenzo,[1] Caralyn Labriola,[1] Lillian Ge,[1] Yan Feng,[1] Zhongming Ge,[1] Vasu Bakthavatchalu,[1] Suresh Muthupalani,[1] Bruce H Horwitz,[2,3] and James G Fox[1,4]

Helicobacter bilis **(Hb) causes hepatitis in some strains of inbred mice. The current study confirmed that Hb directly causes portal hepatitis in outbred gnotobiotic Swiss Webster (SW) mice, as we previously reported for conventional SW mice. Hb-monoassociated SW mice also developed mild enterocolitis, expanded gut-associated lymphoid tissue (GALT), and tertiary lymphoid tissue in the lower bowel. At 1 and 10 mo after infection, Hb-induced GALT hyperplasia exhibited well-organized, ectopic germinal centers with increased mononuclear cell apoptosis, MHC class II antigen presentation, and pronounced endothelial venule formation, consistent with features of tertiary lymphoid tissue. In the lower bowel, Hb induced mainly B220$^+$ cells as well as CD4$^+$IL17$^+$, CD4$^+$IFNγ^+, and CD4$^+$FoxP3$^+$ regulatory T cells and significantly increased *IL10* mRNA expression. This gnotobiotic model confirmed that Hb causes portal hepatitis in outbred SW mice but stimulated GALT with an antiinflammatory bias. Because Hb had both anti- and proinflammatory effects on GALT, it should be considered a 'pathosymbiont provocateur' and merits further evaluation in mouse models of human disease.**

Abbreviations: EHS, enterohepatic *Helicobacter* species; GALT, gut-associated lymphoid tissue; GC, germinal centers; GF, germfree; Hb, *Helicobacter bilis*; Hb-mono, Hb-monoassociated; HEV, high endothelial venules; MLN, mesenteric lymph nodes; mpi, months post infection; SW, Swiss Webster; TBM, tingible body macrophages; TLT, tertiary lymphoid tissue

DOI: 10.30802/AALAS-CM-19-000087

Helicobacter bilis (Hb) is an enterohepatic *Helicobacter* species (EHS) capable of colonizing multiple hosts, including humans, dogs, cats, hamsters, gerbils, mice, and rats, with increasing recognition of systemic disease in immunocompetent subjects.[8,44] Since the first isolation by culture in 1995,[12] Hb and Hb-like organisms[11,17] have been reported to colonize an emerging, ever-widening host range, including evidence of colonization of the human lower bowel associated with enterocolitis[18] and hepatobiliary disease, particularly in patient populations at high risk for gall bladder and biliary tract cancer.[9,28,30,32,35] Unless specifically excluded, Hb is endemic in many rodent breeding colonies[25,39,43] and is a well-established cause of typhlocolitis and colon cancer in immunodeficient mice[13,26,27,31,36] and rats[16] and gastrointestinal lymphomas in hamsters.[46] Similar to *H. hepaticus*, the type EHS species,[16] Hb was isolated from livers with chronic hepatitis in select inbred strains of aged mice,[12,42] presumably due to genetic predisposition. Outbred SW mice used as colony surveillance mice are often infected with Hb and other EHS, but the risk for chronic hepatitis or other adverse effects on research use have been not investigated sufficiently.[39,43,44]

Our discovery of naturally acquired Hb infection associated with liver lesions in outbred Swiss Webster (SW) stock[24] motivated us to confirm direct causality by using gnotobiotic mice. In the current study, germfree (GF) SW mice were monoassociated with Hb and the development of chronic hepatitis was monitored by periodic necropsy over 3 to 14 mo post infection (mpi). Portal hepatitis was observed in aged, primarily female, SW gnotobiotic mice consistent with prior data.[10] In addition, Hb monoassociation concurrently resulted in mild enterocolitis and remarkable gut-associated lymphoid tissue (GALT) hyperplasia with ectopic, tertiary lymphoid tissue (TLT) neogenesis in the cecum and colon. This observation was unexpected and has not been published in regard to Hb or any other helicobacters. We therefore performed a detailed semiquantitative assessment of the effects of Hb on GALT in the absence of other organisms. The effect of Hb on GALT was assessed by colonizing additional GF mice and evaluating GALT at an earlier timepoint (1 mpi) and in chronic stages (10 mpi). To this end, we used quantitative assays that included GALT morphometry, immunohistochemistry, flow cytometry, and quantitative PCR (qPCR) analysis to assess bacterial colonization and mRNA expression of inflammatory and antiinflammatory genes.

Materials and Methods

Ethics statement. The experiments were approved (protocol 1215-115-18) by the Massachusetts Institute of Technology Committee on Animal Care. The facility is AAALAC-accredited and adheres to guidelines published by the Public Health Service in the *Guide for the Care and Use of Laboratory Animals* (8th edition).[19]

Received: 15 Aug 2019. Revision requested: 01 Nov 2019. Accepted: 27 Nov 2019.
[1]Division of Comparative Medicine, Massachusetts Institute of Technology, Cambridge, Massachusetts; [2]Department of Pediatrics, Harvard School of Medicine, Boston, Massachusetts; [3]Department of Pathology, Brigham and Women's Hospital, Boston, Massachusetts; [4]Department of Biological Engineering, Massachusetts Institute of Technology, Cambridge, Massachusetts
[*]Corresponding author. Email: marktwhary@gmail.com
[‡]These authors contributed equally to this study

Score	Description
0	Few to none, small nodular aggregates to scattered cells in either the lamina propria or submucosa (or both).
1	Small numbers of well-spaced, small- to medium-sized discrete mucosal or prominent submucosal (or both) lymphoid aggregates or follicles (or both).
2	Moderate increase in the size and numbers of mucosal or submucosal (or both) lymphoid aggregates or follicles (or both). Add 0.5 for the presence of germinal centers and presence of significant macrophages within follicles or lymphatic engorgement with lymphocytes (or both).
3	Marked increase in the size and numbers of mucosal and submucosal lymphoid follicles, secondary follicle formation, apoptotic or necrotic cells (or both) within activated follicles; germinal centers and secondary follicles present. Increase in plasma cells or macrophages (or both) within lymphoid foci. Lymphatic engorgement with small- to medium-sized lymphocytes. Usually grossly visible (0.1 mm or more in diameter), nodular to granular foci. Add 0.5 for mild cellular atypia with lymphoblast-like features and epitheliotropism.
4	Maltoma, low-grade or high-grade

Figure 1. GALT scoring in cecum and colon. Cumulative maximal score for cecum and colon was 8. Small intestine GALT was minimal and not included in cumulative scores.

Experimental design. ***Experiment 1.*** Over the course of 14 mpi with Hb, 29 GF controls and 36 Hb monoassociated (Hb-mono) SW mice in approximately equal numbers of male and female mice were evaluated histologically for Hb-induced hepatitis, and fecal DNA was probed for Hb colonization through qPCR analysis. The gastrointestinal tracts from 63 of these mice were scored for inflammation and GALT hyperplasia. Livers from a subset of 25 randomly chosen control and Hb-dosed mice were assessed for Hb colonization by qPCR testing. Other livers from control (n = 3) and Hb-dosed mice with the highest histology scores (n = 4) were used for immunohistochemistry to evaluate markers for tertiary lymph node development. To monitor hepatitis, mice were necropsied at 3, 6, 7 through 9, and 11 through 14 mpi. Older mice were clustered in the 7-to-9– and 11-to-14–mpi groups for statistics because data within each cluster were similar.

Experiment 2. An additional 82 male and female mice were used to focus on GALT hyperplasia at an earlier time point (1 mpi) and a late phase (10 mpi). These animals included GF, Hb-mono, SPF control, and Hb-infected SPF SW mice. These mice were used for morphometry of GALT development, immunohistochemistry to identify lymphocyte subsets in enlarged GALT, flow cytometry to quantify lymphocyte subsets in multiple lymphoid tissues, DNA isolation for Hb colonization by qPCR analysis, and RNA isolation to measure cytokine and chemokine expression in multiple tissues.

Bacterial colonization of germfree and specific pathogen-free mice. For Hb colonization, GF and SPF mice were colonized at 6 to 8 wk of age by oral gavage with 200 µL of 10^8 cfu of Hb (Missouri strain; MIT accession 07–9224) on alternate days for 3 doses. Successful colonization of Hb was demonstrated through PCR analysis at several time points after dosing and through necropsy.

Husbandry and health status. GF and gnotobiotic SW mice were maintained in separate plastic-film isolators on autoclaved hardwood bedding in solid-bottomed polycarbonate cages with a 14:10-h light:dark cycle and diet of autoclaved rodent chow (Prolab RMH 3000, PMI Nutrition International, St Louis, MO) and autoclaved water ad libitum. Isolators were sampled every 2 wk and confirmed negative for bacterial and fungal contaminants by culture, fecal Gram stain, and PCR analysis using universal 16S rRNA primers 341F and R806 as previously described to detect all bacteria.[38] SPF mice were naturally colonized with other intestinal bacteria but otherwise were free of exogenous murine viruses, parasites, and bacterial pathogens, including EHS except for mice with experimental Hb infection. Mice were maintained in nonsterile microisolation cages and fed the same autoclaved diet and reverse-osmosis–purified water.

Necropsy. Mice were weighed, scored for body condition, and euthanized through CO_2 overdose. Blood was obtained by the cardiac route and a postmortem gross examination was conducted. Serum, feces, liver, stomach, small intestine, Peyer patches, terminal ileum, cecum, colon, spleen, and mesenteric lymph nodes were collected for RNA, DNA, immunohistochemistry, histology, and flow cytometry. Tissues were opened, rinsed, and laid flat for sectioning into longitudinal strips and then either flash-frozen for RNA isolation (cytokines, chemokines), DNA isolation (qPCR analysis for Hb), placed in glycerol-based freeze media for culture (Hb), or fixed in 10% formalin for histology and immunohistochemistry. For assessment of GALT tissue by using flow cytometry, spleen, mesenteric lymph node, Peyer patches, small intestine, cecum, and colon were collected to prepare single-cell suspensions (see later section). For histology, cecum was collected, and small intestine and colon were Swiss-rolled and fixed in 10% formalin for morphologic assessment. Separate cohorts of mice were used as needed to provide sufficient tissues or single-cell suspensions, and the number of animals used per assay is included in the Results or Figure legends.

Histologic evaluation. Formalin-fixed tissues were routinely processed, embedded in paraffin, cut at 4 µM, stained with hematoxylin and eosin, and evaluated by board-certified veterinary pathologists (VB and SM) who were blinded to sample identity. Cohorts of 10 female and 16 male GF and 22 female and 17 male Hb-mono SW mice (n = 65) were assessed for total hepatitis index. Scores of 0 to 4 for increasing severity of lobular, portal, and interface hepatitis were summed for mice necropsied at 3, 6, 7 to 9, and 11 to 14 mpi, according to our previous report of similar lesions in Hb-colonized conventional SW mice.[10] The small intestine, cecum, and colon were scored for inflammation, edema, epithelial defects, hyperplasia and dysplasia, ranging from 0 (normal) to 4 (extensive, severe) for increasing severity and invasiveness of inflammatory lesions. In addition, 63 of these mice were scored for GALT development (Figure 1) according to qualitative assessment of the small intestine, cecum, and colon for the extent of mononuclear cell infiltrates and hyperplastic lymphoid follicles that first organized as de novo lymphoid aggregates followed by features characteristic of TLT. These features ranged from minimal foci of mononuclear cells to ectopic organized lymphoid tissue that demonstrated stromal compartmentalization of B and T cells organized around high endothelial venules (HEV; Figure 1).

GALT morphometry was performed on an additional 43 male and 39 female mice at 1 and 10 mpi by using previously published criteria.[3,4,6,7,21-23,29] Longitudinal sections of the cecum and colon were quantitatively assessed by a board-certified

Table 1. Liver scores (median [range]) in a subset of aged GF controls and Hb-mono Swiss Webster mice at 13 to 14 mpi

	Hepatitis index (scale, 0–12)	Lobular (scale, 0–4)	Portal (scale, 0–4)	Interface (scale, 0–4)	Lobes with > 5 foci
GF control males (n = 4)	0.75 (0–1)	0.5 (0–0.5)	0 (0–0.5)	0 (0)	0 (0)
GF control females (n = 4)	0.75 (0–1)	0.5 (0–0.5)	0 (0–0.5)	0 (0)	0 (0)
Hb-mono males (n = 4)	1 (0–1)	0.75 (0–1)	0 (0–0.5)	0 (0)	0 (0)
Hb-mono females (n = 8)	3.25 (0.5–7.5)[a]	0.5 (0–2)	1 (0.5–2.5)[b]	0 (0–1)	1 (0–4)

[a]$P < 0.001$ compared to all groups.
[b]$P < 0.05$ compared to all groups.

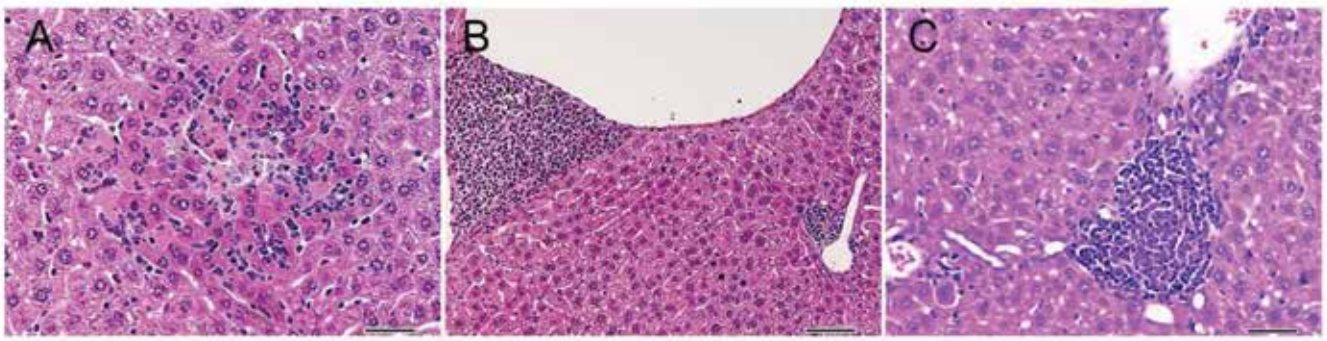

Figure 2. Representative hepatic lesions observed in Hb-mono mice. (A) Lobular pattern of hepatitis. (B) Portal activity. (C) Perivenular mononuclear cell foci. Magnification, 400×.

Table 2. Combined cecum and colon scores (median [range]) for enterocolitis and GALT hyperplasia

	Enterocolitis				GALT hyperplasia	
	Inflammation (scale, 0–4)	Edema (scale, 0–4)	Epithelial defects (scale, 0–4)	Total score (scale, 0–12)	GALT score (scale, 0–8)	n
GF control						
3 mpi	0.25 (0–1.5)	0 (0–0.5)	0.25 (0–1.5)	0.75 (0–3.5)	1 (0.5–1)	8
6 mpi	0.5 (0–1.5)	0.25 (0–2)	0.5 (0–1.5)	1 (0–4.5)	1.5 (0–2)	8
7–9 mpi	1.25 (0–2)	0 (0–1)	1 (1–2)	2.75 (1–4)	2.25 (1.5–3)	6
11–14 mpi	1 (0–1)	0.5 (0–0.5)	1.5 (1–2)	3 (1–3)	2 (1.5–3)	7
Hb-mono						
3 mpi	1.5 (0–2.0)[b]	0.5 (0–1.5)[b]	1 (0–1.5)	2.75 (1.5–5)[b]	3.5 (1–4.5)[b]	8
6 mpi	1.75 (1–2.5)[b]	1 (0–1.5)	0 (0.75–1.5)	3.5 (1.5–5)[a]	4 (3–5)[b]	8
7–9 mpi	1.5 (1–2.5)	0.5 (0–1.5)	1 (0.5–2)	3 (2–5.5)	4.5 (3.5–6)[c]	13
11–14 mpi	1.75 (0.5–2.5)[a]	0.25 (0–1.5)	1 (0.5–3)*	2.75 (1–8)	4.5 (2–5.5)[b]	12

[a]$P < 0.05$, [b]$P < 0.01$, [c]$P < 0.001$ regarding comparison of controls with Hb-mono mice at respective time points.

veterinary pathologist (VB) blinded to the sample identity. cellSens imaging software (Olympus Life Sciences, Waltham, MA) was used to quantify the number and size of lymphoid aggregates. Total lymphoid aggregate area and the number, size, and total area of GC were measured along with the ratio of activated GC to lymphoid aggregates. As biomarkers for GC activation, well-defined lymphoid aggregates were counted and then assessed qualitatively for extent of apoptosis and relative number of associated tingible body macrophages, which clear lymphoid tissues of dead cells.[6] Additional biomarkers included prominent HEV and ectatic lymphatic vessels engorged with mononuclear cells morphologically similar to cellular infiltrates in the lamina propria. Data regarding the absolute number, average size, and total area of lymphoid aggregates and GCs are presented for the colon, because of the uniform length of Swiss-roll sections. Sections of cecum were more variable in length, so the data are presented as the ratio of GC to lymphoid aggregates and the percentage of GC that met criteria for activation. Data were combined to include cecal and colonic assessments as appropriate and are so indicated in the figure legends.

Immunohistochemistry. For assessment of B cell, T cell, and macrophage contributions to TLT development, formalin-fixed sections from the ileocecal–colic junction were evaluated from 3 GF and 3 Hb-mono mice at 9 mpi. Antibodies included those to CD3 (pan-T-cell marker using rabbit polyclonal antihuman CD3, catalog no. AO452, Dako, Santa Clara, CA), CD45/B220 (pan-B-cell marker using rabbit polyclonal, cat. no. ab10558, Abcam, Cambridge, MA), F4/80 (macrophage marker using rat monoclonal, cat. no. MF48015, Caltag Medsystems, Buckingham, United Kingdom) and Ki67 nuclear protein (cell proliferation) by using mouse antihuman antibody (catalog no. 550609, BD Biosciences, Franklin Lakes, NJ). Liver sections from 3 GF controls and 4 Hb-mono female mice with the highest liver lesion scores at 11 to 14 mpi were processed similarly. Staining was performed according to previously described methods for antigen retrieval, blocking, and counterstaining.[34] $CD3^+$ or $B220^+$ cells that were colocalized on serial tissue sections with Ki67

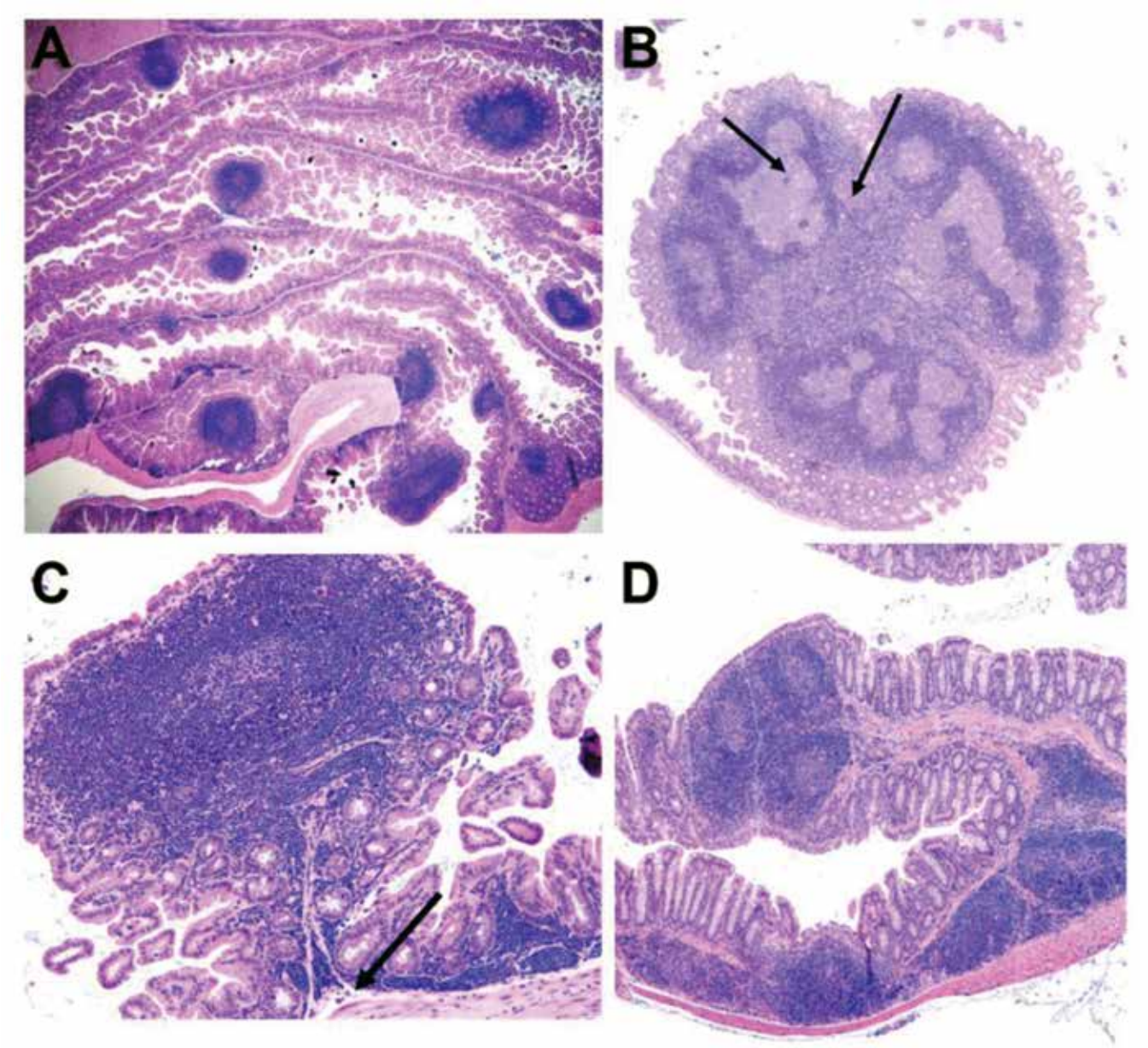

Figure 3. Hb-mono SW mice demonstrated significant expansion of GALT when assessed at 3, 6, 9, and 11–14 mo post Hb colonization (mpi). Representative sections of the cecum and ileocecal–colic junction at 9 mpi show (A) prominent lymphoid structures that morphologically are similar to (B) lymph nodes with follicular areas (left arrow) surrounding germinal centers (right arrow) in the cecum. (C) Note lymphatic engorgement with mononuclear cells (arrow). (D) GALT was hypertrophied in the colon also. Magnification, 20× (A and D), 100× (B and C).

nuclear-positive cells were considered activated and proliferating.

Immunohistochemistry was performed on Swiss-roll sections of colon from 3 GF and 3 Hb-mono mice 1 mpi. Tissues were stained for caspase III (rabbit monoclonal Asp175, clone 5A1E, Cell Signaling Technology, Danvers, MA), mucosal addressin cell adhesion molecule (MAdCAM) lymph node addressin (rat monoclonal MECA79 from Santa Cruz Biotechnology), and MHC class II (rat monoclonal ab139365, Abcam, Cambridge, MA). Buffers, blocking reagents, secondary antibodies, and DAB chromagen were supplied by Biocare Medical (Concord, CA) and used with hematoxylin counterstain in a Varistain 24 autostainer (Thermo Fisher Scientific, Waltham, MA).

Cell isolation, stimulation and flow cytometry. Single-cell suspensions were isolated from mesenteric lymph nodes, Peyer patches, and spleens by disassociating tissues through 75-µm cell strainers (Thermo Fisher Scientific) as previously described.[41] Mononuclear cells from intestinal lamina propria were isolated with RPMI 1640 solution containing collagenase (C2139, Sigma–Aldrich, St Louis, MO) after 3 to 5 incubations in EDTA-supplemented Hanks Balanced Salt Solution followed by filtering through 75-µm cell strainers. For B- and T-cell surface staining, single-cell suspensions were labeled with antimouse B220 (clone RA3-6B2, BioLegend, Dedham, MA) and antimouse CD4 (clone RM4-5, BioLegend) at 4 °C for 30 min with predetermined concentrations. Intracellular cytokine staining for IL17 (TC11-18H10.1, BioLegend) and IFNγ (XMG1.2) protein were performed after cell activation with phorbol 12-myristate 13-acetate (50 ng/mL; Sigma–Aldrich) and ionomycin (1 µg/mL) for 4 h at 37 °C in the presence of monensin (10 µg/mL). Cells isolated from various organs were stained for surface expression of CD4 (clone RM4-5; BioLegend) and CD44 (clone

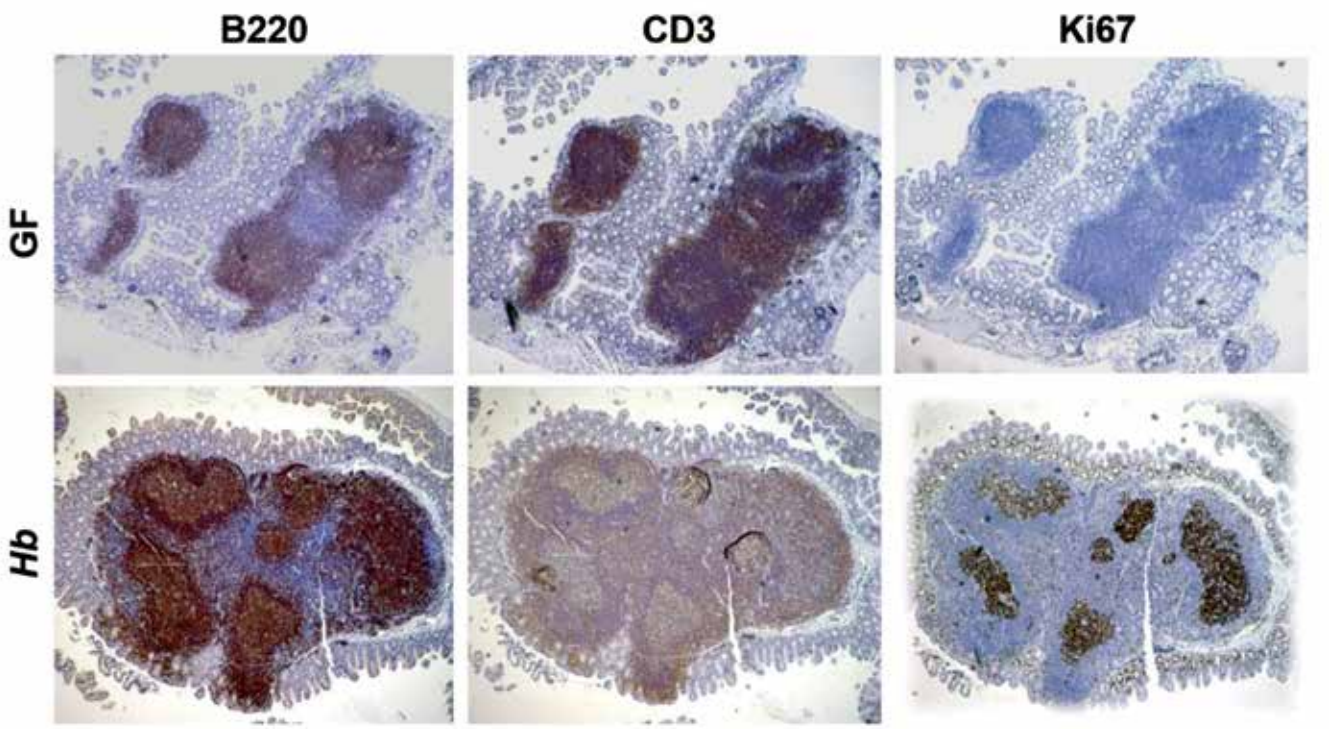

Figure 4. Immunohistochemistry of serial sections of morphologically well-defined tertiary lymphoid tissues isolated from the ileocecal-colic junction for B220, CD3, and Ki67. Germfree controls (GF) (top row) and Hb-mono mice (bottom row). Staining patterns are representative of 3 GF and 3 Hb-mono mice at 9 mpi.

IM7; BioLegend). After fixation and permeabilization, cells were stained for FoxP3 (clone FJK-16s, eBioscience, San Diego, CA) according to the manufacturer's protocol. Absolute cell numbers for each flow cytometry marker were calculated as total cells analyzed multiplied by the percentage of cells positively stained. Stained cells were acquired by using an LSR Fortessa flow cytometer (BD Biosciences) and analyzed with FlowJo 10.1 software (Tree Star, Ashland, OR).

mRNA expression levels. Tissues for RNA isolation were snap-frozen in liquid nitrogen and stored at −80 °C prior to processing. For relative mRNA quantitation of selected genes, total RNA from cecum and colon was prepared by using Trizol (Invitrogen, Carlsbad, CA) according to the manufacturer's directions. Total RNA (5 µg) from each sample was reverse-transcribed to cDNA by using High-Capacity cDNA Archive kit (Applied Biosystems, Foster City, CA) according to manufacturer's instructions. mRNA transcript levels of *CXCL13*, *CCL21*, *LT*β, *IFN*γ, *IL1*β, *IL17*, and *IL10* were measured through qPCR analysis using commercial primers and probes (TaqMan Gene Expression Assays) in the ABI Prism 7500 FAST Sequence Detection System (Life Technology, Foster City, CA). Transcript levels were normalized to endogenous control glyceraldehyde-3-phosphate dehydrogenase (*GAPDH*) mRNA and expressed as fold change compared with control mice according to the comparative C_t method (User Bulletin No. 2, Applied Biosystems).

***H. bilis* PCR and qPCR analysis.** Total DNA from intestinal tissues and fecal samples was prepared by using High Pure PCR Template Preparation Kit (Roche Diagnostics, Indianapolis, IN) and the QIAamp Fast DNA Stool Mini Kit (Qiagen, Valencia, CA) according to the suppliers' protocols. qPCR assays were performed in the 7500 Fast Real-Time PCR System. Levels of Hb in cecal and colonic samples were measured by using the Hb 16S rRNA gene-based primers and the fluorogenic probe previously described.[5] PCR assays for Hb in liver samples harvested through 14 mpi were screened by standard PCR analysis as previously published.[10]

Statistical analysis. Hepatitis and GALT scores were compared by the nonparametric Kruskal–Wallis test followed by Dunn pairwise comparisons and Mann–Whitney nonparametric comparisons. GALT morphometry, flow cytometry, bacterial colonization, and mRNA expression data were compared by using one-way ANOVA and unpaired Student *t* tests, with Welch correction for potentially unequal variances. Potential effects attributed to sex were determined by logistical regression by using Excel (Microsoft, Seattle, WA). Female mice were predisposed to hepatitis, but gastrointestinal assays were similar between males and females. The balance of statistical analysis was performed by using Prism 5.0 (GraphPad Software, La Jolla, CA), with *P* values less than 0.05 considered significant.

Results

Portal hepatitis. We previously reported that chronic, active hepatitis was associated with Hb in aged outbred SW mice that were colonized with conventional microbiota.[10] To demonstrate direct causation, GF SW mice were monoassociated with Hb and monitored for chronic hepatitis over 14 mpi. Hepatic lesions predominantly involved mononuclear cell infiltrates in the portal triad, particularly in older female mice at 13 to 14 mpi (Table 1, Figure 2 A). Scores for lobular and interface hepatitis were low and not significantly different between GF and Hb-mono mice. No significant liver lesions were detected in mice younger than 9 mpi. Compared with GF control mice, Hb-mono mice aged 9 to 14 mpi showed some perivenular mononuclear cell aggregates in multiple liver lobes from 2 of 10 male mice and 8 of 15 female mice (Figure 2 B and C). Immunohistochemistry identified moderate numbers of B and T cells but minimal to no staining for biomarkers of activated TLT, as shown for

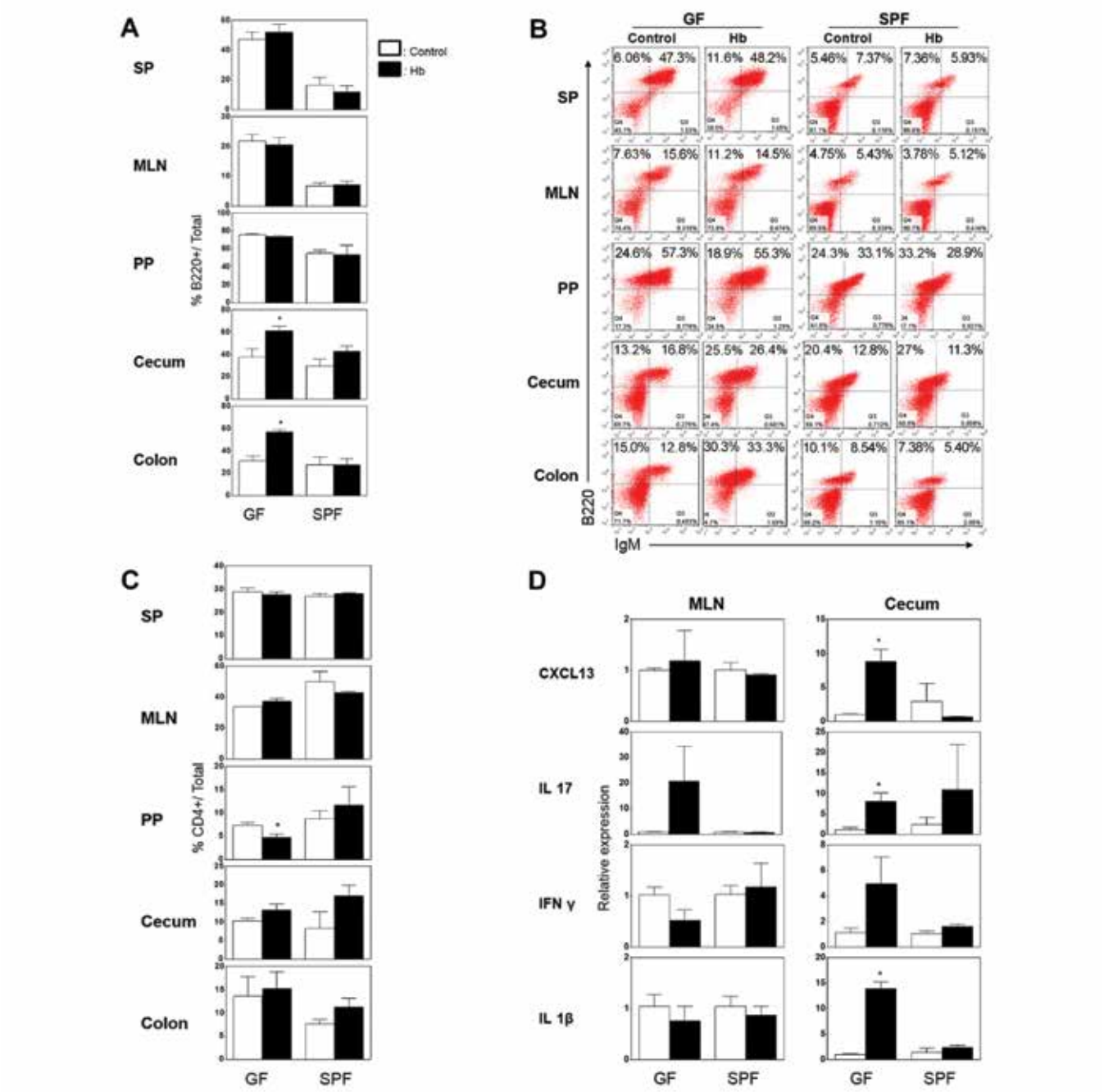

Figure 5. Flow cytometry measured (A and B) B220⁺ cells, (C) CD4⁺ cells, and (D) cytokines and chemokines in response to Hb colonization. Data represent the spleen (SP), mesenteric lymph nodes (MLN), small intestinal Peyer patches (PP), and the lamina propria (LP) of cecum and colon harvested from GF, Hb-mono, SPF, and Hb infected SPF mice in groups of 3 mice at 1 mpi. *, $P < 0.05$.

GALT tissues (see Results). These included cleaved intracellular caspase 3 as evidence of apoptosis, cell surface expression of MHC class II signifying antigen presentation and cell activation, and for HEV expressing addressin. Consistent with our prior observations of minor liver lesion scores, PCR analysis for Hb colonization of the liver was negative in a sampling of 25 mice even though feces and cecal tissues were qPCR-positive for Hb, with colonization levels approximating 10^6 to 10^7 cfu per µg host DNA.

GALT hyperplasia. A standardized approach for scoring EHS-mediated enterocolitis in mouse models [1] was used to perform histologic evaluation of the small intestine, cecum, and colon of control GF and Hb-mono SW mice (Table 2). Scores were assigned for inflammation, edema, and epithelial defects; other features such as crypt atrophy and epithelial hyperplasia and dysplasia were not observed. Because neither inflammatory infiltrates nor organized lymphoid tissue other than Peyer Patches developed in the small intestine of Hb-mono mice, only cecum and colon scores were combined into total scores. Hb-mono mice had higher scores for enterocolitis, primarily attributable to mild inflammation, compared with control GF mice at 3 and 6 mpi. In addition, submucosal edema was greater in Hb-mono mice at 3 mpi, and epithelial defects were greater than GF controls at 11 to 14 mpi. Enterocolitis over time was sufficiently mild that scores at 7 to 9 mpi and 11 to 14 mpi were similar between control GF and Hb-mono mice.

Table 3. Numbers (×10⁶; mean ± SE) of B220⁺ and CD4⁺ cells harvested from GALT of GF controls, Hb-mono (Hb), SPF, and Hb-infected SPF Swiss Webster mice at 1 mpi

	GF	Hb	SPF	Hb SPF
B220⁺ cells				
Spleen	13.35 ± 3.40	14.75 ± 3.02	3.24 ± 1.37	2.47 ± 1.38
MLN	3.07 ± 0.67	3.77 ± 0.77	0.30 ± 0.07	0.68 ± 0.19
Peyer patches	2.13 ± 0.66	0.86 ± 0.11	4.15 ± 0.66	3.02 ± 1.02
Cecum	0.48 ± 0.12	3.78 ± 0.87*	1.11 ± 0.16	2.58 ± 0.64
Colon	0.80 ± 0.37	3.95 ± 1.36	1.03 ± 0.15	0.97 ± 0.21
CD4⁺ cells				
Spleen	6.65 ± 1.05	6.66 ± 0.97	5.22 ± 0.78	5.07 ± 1.07
MLN	4.30 ± 0.53	6.89 ± 0.29	2.73 ± 1.36	3.89 ± 0.41
Peyer patches	0.17 ± 0.06	0.05 ± 0.01	0.69 ± 0.20	0.72 ± 0.31
Cecum	0.17 ± 0.02	0.79 ± 0.26	0.29 ± 0.15	1.03 ± 0.30
Colon	0.43 ± 0.24	1.37 ± 0.70	0.30 ± 0.51	0.41 ± 0.07

Data support Figure 5. $n = 3$ per group.
[a]$P < 0.05$ regarding comparison of control GF and SPF mice with Hb-mono and Hb-infected SPF mice, respectively.

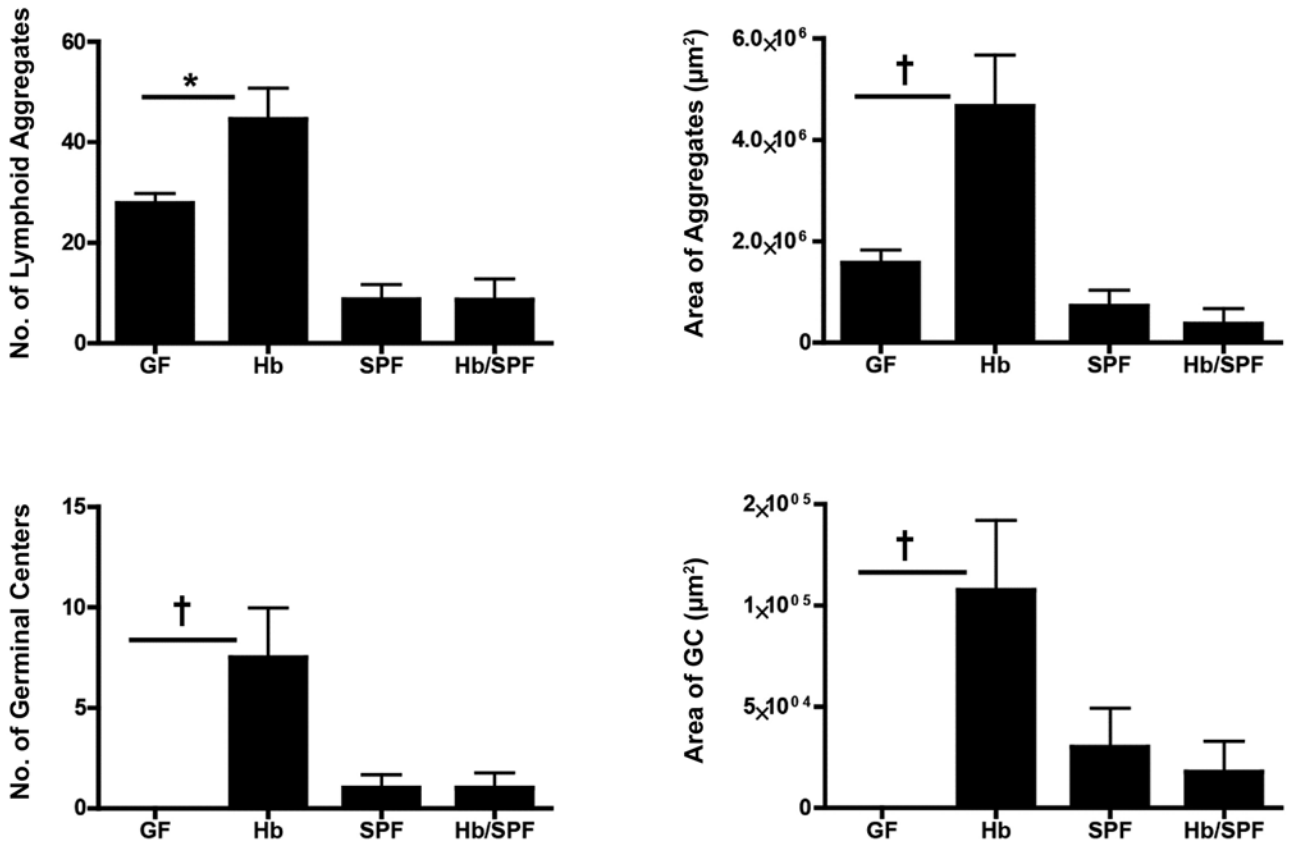

Figure 6. Numbers and areas (mean ± SE) of lymphoid aggregates and germinal centers (GC) measured by morphometry of colon sections at 10 mpi. GF, $n = 6$; Hb-mono, $n = 10$; SPF, $n = 6$; and Hb-infected SPF, $n = 5$. *, $P < 0.05$; †, $P < 0.01$; ‡, $P < 0.001$.

GALT hyperplasia in the cecum and colon was first assessed at 3 mpi. GALT scores for Hb-mono mice were higher than GF mice at each time point from 3 mpi through 11 to 14 mpi; scores for Hb-mono mice peaked at 6 mpi and remained elevated through 11 to 14 mpi. Hb-mono mice developed a range of ectopic lymphogenesis in the lamina propria of the cecum and colon, varying from cryptopatches of mononuclear cells to larger, isolated lymphoid follicles, some of which were macroscopically visible and characteristic of TLT, with lymph node architecture (Figure 3 A and B). GF control tissues contained small, scattered lymphoid aggregates but lacked evidence of organized lymphoid tissues resembling TLT. The ileocecal–colic junction and colon in Hb-mono mice had mature follicles with well-demarcated GC (Figure 3 B). No mice had high GALT scores characteristic of lymphoma of mucosa-associated lymphoid tissue. Ectatic (engorged) lymphatics in the lamina propria contained mononuclear cells trafficking to the organized lymphoid structures (Figure 3 C). GALT expansion was most prominent at the ileocecal-colic junction (Figure

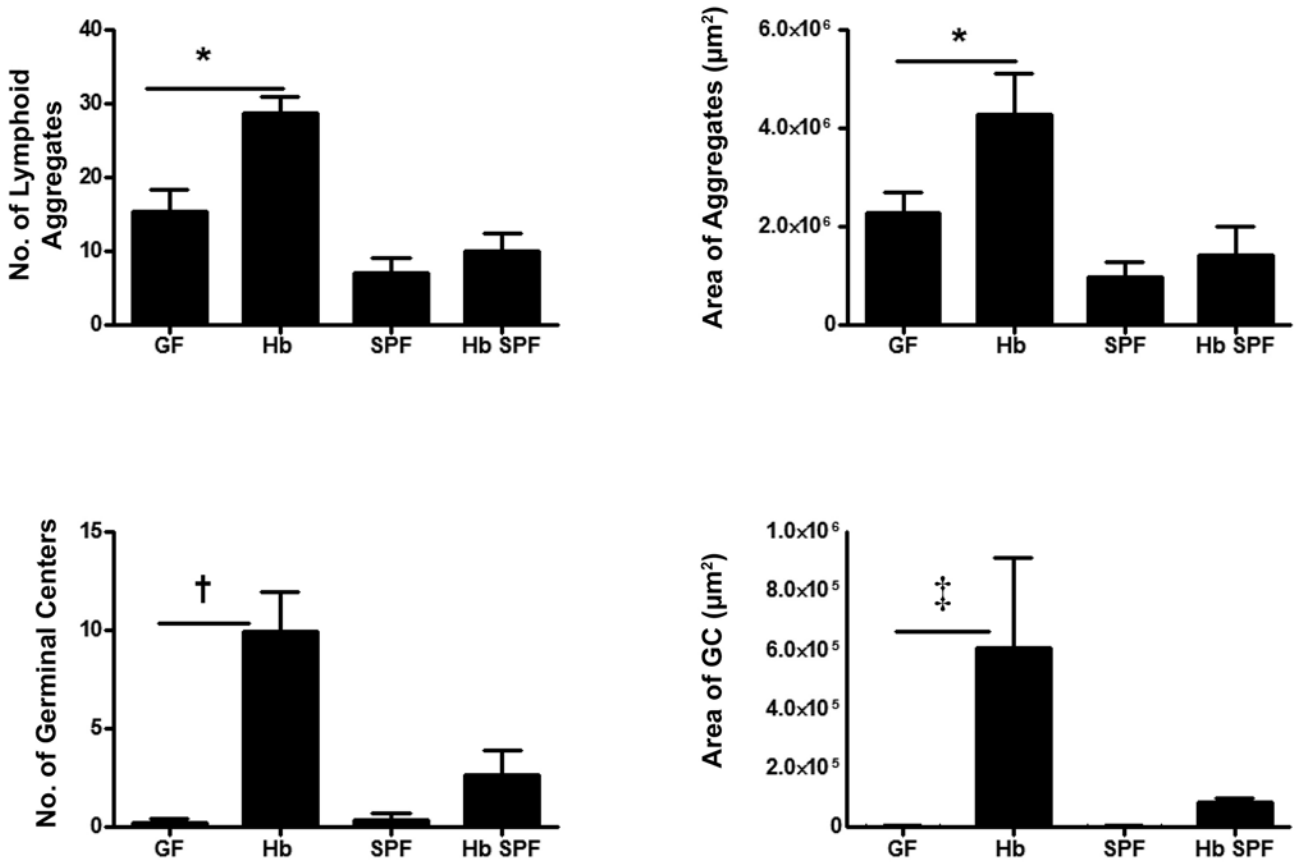

Figure 7. Numbers and area (mean ± SE) of lymphoid aggregates and germinal centers (GC) measured by morphometry in colon sections at 1 mpi. GF, n = 10; Hb-mono, n = 10; SPF, n = 3; Hb-infected SPF, n = 3. *, P < 0.05; †, P < 0.01; ‡, P < 0.001.

3 D), the preferred niche for Hb colonization. Hb-specific qPCR analysis demonstrated a mean of 10^6 Hb copies per µg of host DNA at the ileocecal–colic junction in 4 female and 4 male Hb-mono mice necropsied at 6 mpi. Hb copy number was 1 log lower in the colon and several logs lower in the small intestine.

Immunohistochemistry of TLT in sections of the ileocecal–colic junction of GF mice had moderate staining intensity for the pan-B cell marker $B220^+$, T cell $CD3^+$, and the cell proliferation marker Ki67 (Figure 4). Similar tissue sections of TLT from Hb-mono mice had well-defined lymphoid aggregates and follicles characteristic of TLT at the ileocecal–colic junction and stained intensely for B220 and Ki67. Small numbers of parafollicular $CD3^+$ cells surrounded these $B220^+$-enriched follicles and these $CD3^+$ cells had less intense staining for Ki67. $F4/80^+$ macrophages and neutrophils were not observed in significant numbers in sections from either GF or Hb-mono mice.

Expanded GALT with morphologically well-developed GC in Hb-mono mice was further documented and expanded in additional experiments that used an earlier time point (1 mpi) for phenotyping cell types and associated cytokines and chemokines. Preliminary measurements of select mRNA expression levels and flow cytometry phenotyping on single-cell suspensions from the spleen, mesenteric lymph nodes, small-intestinal Peyer patches, and the lamina propria of the cecum and colon were performed. Compared with GF mice, Hb-mono mice showed significant increases in the percentage and absolute number of $B220^+$ cells in the lamina propria of the cecum, with a similar trend for increased $B220^+$ cells in the colon (Figure 5 A, Table 3). As a gauge of early humoral immunity, the percentage of mononuclear cells double-positive for $B220^+$ and IgM^+ in cecum increased from 16.8% in GF to 26.4% in Hb-mono mice and in colon from 12.8% in GF to 33.3% in Hb-mono mice (Figure 5 B). Although the absolute number of $CD4^+$ cells trended higher in the mesenteric lymph nodes (MLN), cecum, and colon of Hb-mono and Hb-infected SPF mice (Table 3), the $CD4^+$ cell percentage of total cells did not significantly differ between GF, Hb-mono, SPF, and Hb-infected SPF mice (Figure 5 C). mRNA expression levels for *CXCL13*, *IL17*, and *IL1*β were significantly higher in the cecum of Hb-mono mice and accompanied a trend for increased expression of *IFN*γ mRNA (Figure 5 D). No significant changes in these markers were detected in Hb-infected SPF mice (Figure 5).

In the third experiment, GALT hyperplasia persisted in Hb-mono mice at 10 mpi, as noted in a prior 14-mo experiment There was a persistent increase in the number and area of lymphoid aggregates and GC attributable to Hb (Figure 6). The Hb-infected SPF mice at 10 mpi did not have significant GALT hyperplasia, confirming the utility of the Hb-mono gnotobiotic model to study the effects of Hb on GALT.

GC in the cecum and colon. Differentiation and activation of GC were estimated first by morphometric assessment of the lymphoid aggregates in cecum and colon that had well-defined GC (Figure 7). Hb significantly increased the number and area of lymphoid aggregates and GC in Hb-mono mice. Immunohistochemistry and staining with hematoxylin and eosin were used to confirm that hyperplastic GALT had features of TLT, including apoptotic cells, tingible body macrophages, HEV, and ectatic lymphatics, as used by others.[3,4,6,7,21-23,29] Sections from the ileocecal-colic junction were stained for cleaved caspase 3 as a

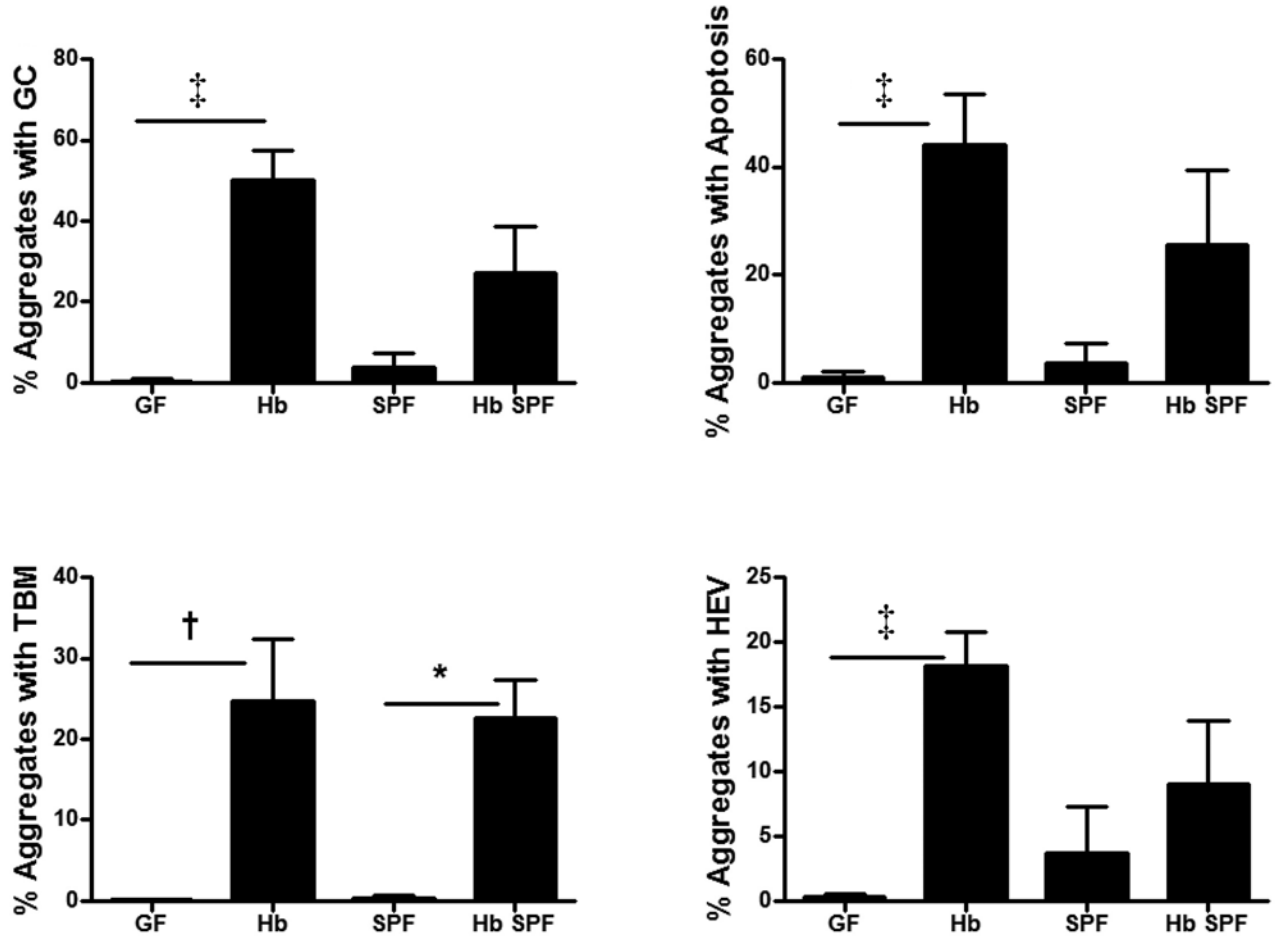

Figure 8. Percentage (mean ± SE) of lymphoid aggregates in cecum and colon that developed germinal centers (GC) by 1 mpi and the percentages of aggregates with apoptosis, tingible body macrophages (TBM), and high endothelial venules (HEV). GF, $n = 10$; Hb-mono, $n = 10$; SPF, $n = 3$; Hb-infected SPF, $n = 3$. *, $P < 0.05$; †, $P < 0.01$; ‡, $P < 0.001$.

marker for the apoptotic signaling pathway, MHC class II for antigen presentation, and MECA79 for endothelial staining of HEV.

Hb monoassociation significantly increased the percentage of lymphoid aggregates in the cecum and colon, with enhanced immune activation as defined by increased numbers of apoptotic cells, tingible body macrophages, and HEV (Figure 8). Ectatic lymphatics are evidence of increased lymphocyte traffic; the percentages (mean ± SE) of these in the cecum and colon were highest in Hb-mono mice (21% ± 5%). In contrast, GF mice had low numbers of ectatic lymphatics (8% ± 3%); $P < 0.04$), which were similar in Hb-infected SPF mice (10% ± 10%; Figure 8).

Compared with control GF SW mice (Figure 9 A), hematoxylin and eosin staining demonstrated that GALT hyperplasia was most dramatic for Hb-mono mice (Figure 9 B). GALT from GF mice did not stain for cleaved caspase 3 (Figure 9 C) and stained only modestly for MHC class II (Figure 8 E) and MECA79 (Figure 9 G). The numbers of cells stained with cleaved caspase 3, MHC class II, and MECA79 were all greater in Hb mice (Figure 9 D, F, and H). Notably, mononuclear cells migrating through the ectatic lymphatics of Hb-mono mice had high expression of MHC class II antigens.

At 10 mpi, experimental groups included GF, Hb-mono, SPF, and Hb-infected SPF mice. The percentages of lymphoid aggregates in the cecum and colon that had morphologically well-defined GC remained higher in Hb-mono mice compared with the relative absence of lymphoid aggregates and GC in GF and SPF mice with or without Hb colonization (Figure 10). The GALT-stimulating features of Hb were less intense compared with those observed at 1 mpi (Figure 8), but the increases in lymphoid aggregate number and area and in the number and total GC area were similar. At 10 mpi, the percentage of aggregates with well-differentiated and activated GC was approximately 33% to 50% lower in Hb-mono mice compared with the same group at 1 mpi. The percentage (mean ± SE) of lymphoid aggregates in the cecum and colon with ectatic lymphatics continued to be highest in Hb-mono mice (16% ± 6%) compared with GF mice (2% ± 2%; $P < 0.04$), which were equivalent to SPF mice (6% ± 6%). No engorged lymphatics were observed in Hb-infected SPF mice.

Cells involved in GALT hyperplasia. Flow phenotyping of single-cell suspensions from MLN, small intestine, cecum, and colon measured Hb promotion of $B220^+CD4^+$ cells and subsets of $CD4^+$ cells that were $IL17^+$, $IFN\gamma^+$, and $FoxP3^+$ (Figure 11).

At 1 mpi, Hb did not alter $B220^+$ cell numbers in MLN. $B220^+$ cell numbers increased in the SI of Hb-mono mice. Similarly, $CD4^+$ counts trended higher in small intestine with Hb colonization. Hb increased $B220^+$ cells in the lower bowel approximately 5-fold compared with lower increases in $CD4^+$ cells.

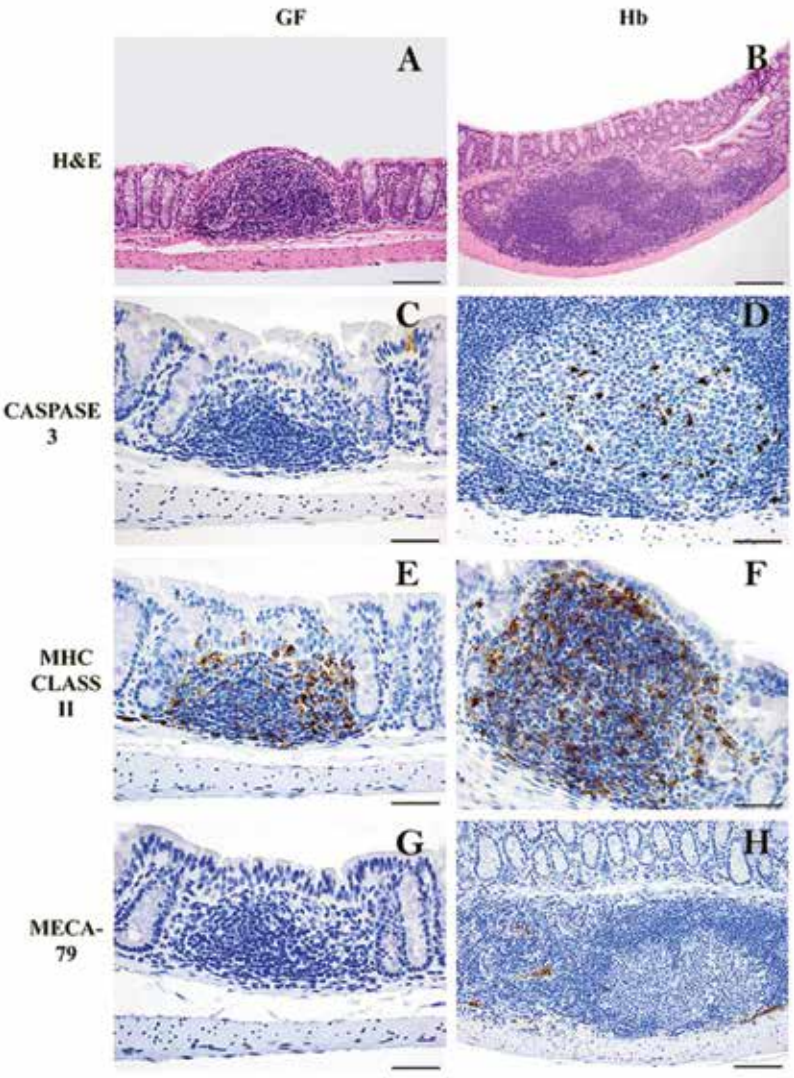

Figure 9. Representative colon sections from GF and Hb-mono SW mice at 1 mpi. (A) Rare GALT in GF mice, with absence of GC. (B) Increased number and size of germinal centers in Hb-mono mice (bar, 100 µm). (C and D) Increased staining for cleaved caspase 3 in Hb-mono compared with GF mice (bar, 50 µm). Increased staining for (E and F) MHC class II and (G and H) MECA79 (MAdCAM) in endothelial cells of Hb compared with GF mice. Hematoxylin and eosin staining (H&E) or immunohistochemistry.

Although total $CD4^+$ cell counts in MLN did not change in Hb-colonized mice, Hb promoted the subset of $CD4^+IL17^+$ cells in MLN. The $CD4^+IL17^+$ counts in the small intestine of Hb-colonized mice trended higher but became significant in the cecum and colon, in which Hb increased $CD4^+IL17^+$ counts to a similar extent in both tissues. MLN from all groups of mice had similarly low $CD4^+IFN\gamma^+$ cell counts. Hb monoassociation promoted these cells in the small intestine. Hb significantly increased the numbers of $CD4^+IFN\gamma^+$ cells in cecum and colon. $CD4^+FoxP3^+$ cell counts in MLN did not vary, although all Hb-mono mice had more of these regulatory T cells in small intestine and cecum than other groups.

The 10-mpi time point included evaluation of the same cell subsets from GF and Hb-mono mice. Persistence of $B220^+$ cell expansion in response to Hb monoassociation was observed at 10 mpi in cecum with approximately 5-fold higher levels than GF controls (Table 4). $CD4^+$ cells were slightly increased in small intestine and were 5-fold higher in the cecum of Hb-mono mice. Hb increased the number of $CD4^+IL17^+$ in the cecum and $CD4^+IFN\gamma^+$ and $CD4^+FoxP3^+$ regulatory T cells in the lamina propria of small intestine, cecum, and colon, consistent with similar changes observed at 1 mpi (Table 4).

mRNA expression of chemokines and cytokines important for limiting enterocolitis and supporting GALT hyperplasia. mRNA was isolated from spleen, MLN, cecum, and colon for measuring expression levels of *CXCL13*, *CCL21*, *LT*β, *IFN*γ, *IL17*, and *IL10* at 1 and 10 mpi. Hb colonization was associated with lower *CXCL13* transcription levels in spleen (Figure 12) but with higher *CXCL13* transcription in cecum and colon. *CCL21* mRNA levels were increased by Hb colonization in the spleen and colon. *LT*β expression levels were lower in spleen and MLN but higher in cecum and colon from mice infected by Hb. Hb significantly stimulated *IFN*γ mRNA expression in the cecum but not the colon. Hb increased expression of *IL17* mRNA in MLN and colon. *IL10* expression was markedly enhanced in cecum and colon by Hb.

The patterns of Hb-enhancing mRNA expression at 1 mpi persisted through 10 mpi (Figure 13), with the exception of *CCL21*, which was unchanged. Hb monoassociation significantly

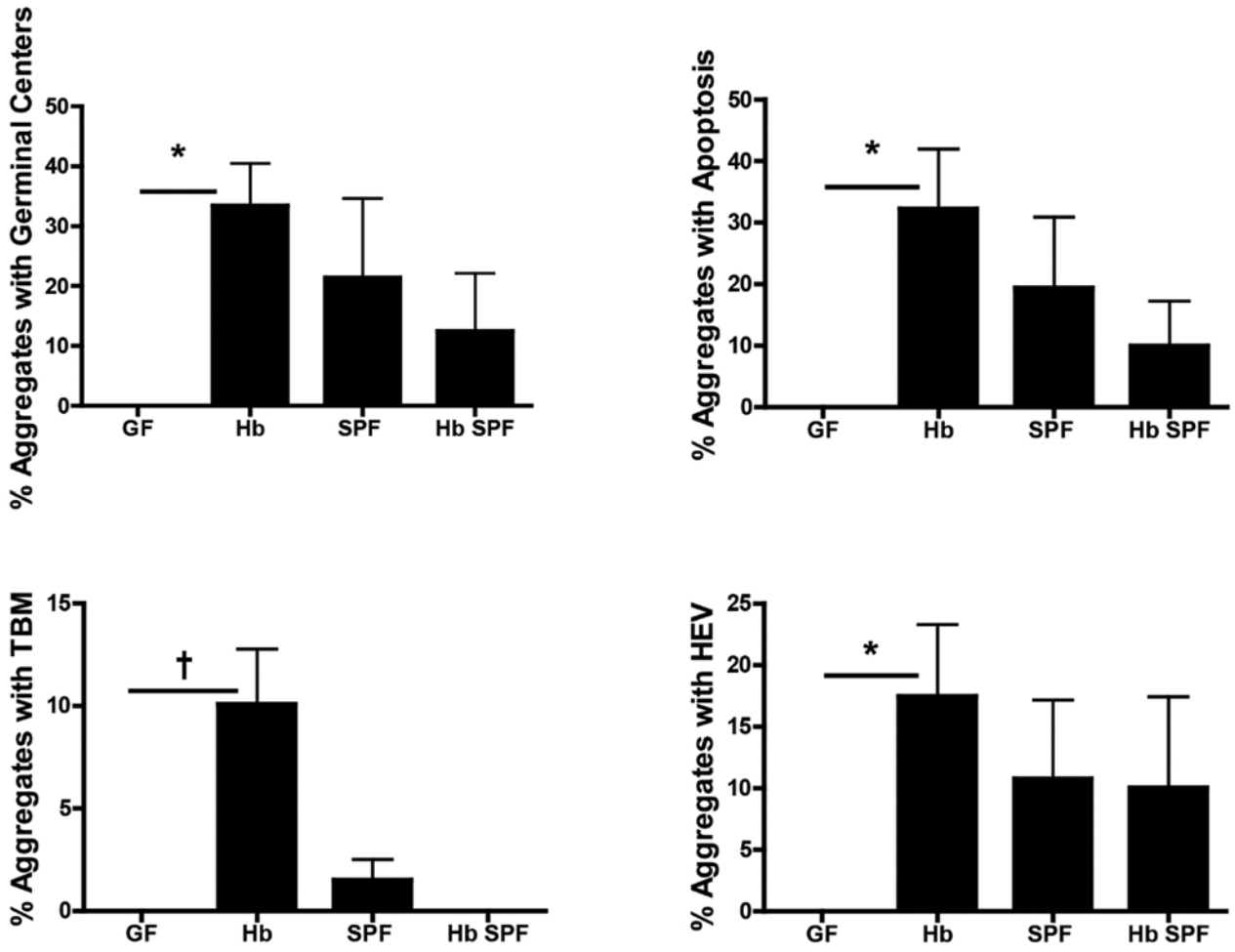

Figure 10. Percentages (mean ± SE) of lymphoid aggregates in the cecum and colon at 10 mpi that developed well-defined germinal centers, apoptosis, tingible body macrophages (TBM), and high endothelial venules (HEV) in GF (n = 7), Hb-mono (n = 10), SPF (n = 9), or Hb-infected SPF (n = 5) mice. *, $P < 0.05$; †, $P < 0.01$; ‡, $P < 0.001$..

increased *CXCL13*, *LT*β, *IFN*γ, *IL17* and *IL10* in either the cecum and / or colon. Hb also had a significant promotion of *IL17* in the spleen.

Discussion

Helicobacter hepaticus–associated chronic active hepatitis has been described in aged, inbred mice (predominantly males).[12,42] Our current study confirmed that Hb-induced hepatitis can develop in aged outbred SW mice. Lesions were noted predominately in female mice, a signalment consistent with our previous report in conventional SW mice.[10] Before hepatitis developed, young adult Hb-mono mice of both sexes developed low-grade enterocolitis accompanied by progressive GALT hyperplasia that persisted essentially for the animal's life. Hb stimulated TLT neogenesis with lymph node architecture in cecum and colon, along with significant GC activation. Hb had both anti- and proinflammatory effects on GALT. Hb induced primarily an antiinflammatory tissue environment attributable to increased $CD4^+FoxP3^+$ regulatory T cells and enhanced *IL10* mRNA expression, thus contrasting with the typical notion of Hb as a pathogen in immunocompromised mice. To our knowledge, neither GALT hyperplasia in the lower bowel nor development of TLT attributable to infection with murine EHS in outbred SW mice has been reported previously. Outbred SW mice are not commonly used in research in infectious diseases and immunology, and necropsy evaluation is often less comprehensive compared with inbred mice and may account for occult hepatitis or other effects of EHS infection such as GALT hyperplasia being overlooked.

Koch postulates were successfully achieved, given that Hb monoassociation caused chronic portal hepatitis in outbred SW mice. Clearly the gnotobiotic model demonstrates definitive causation from Hb infection rather than the simple association that can be achieved when studied in conventional mice with a complex microbiota. In our study, the portal lesions were mild and not observed in all mice, consistent with the historical resistance of outbred mice to EHS-mediated hepatitis. Hb induction of elevated *IL10* mRNA expression and increased numbers of $CD4^+FoxP3^+$ regulatory cells in the lower bowel may impart a decreased 'off-shore' inflammatory effect in the liver. As we previously reported in conventional mice,[10] liver lesions developed primarily in aged, female Hb-mono mice. Further studies to define the sex-associated bias are needed. Portal hepatitis could not be definitively associated with active Hb liver infection at the time of necropsy, consistent with prior clearance.

Table 4. Numbers (mean ± SE) of $B220^+$, $CD4^+$, $CD4^+IL17^+$, $CD4^+IFN\gamma^+$, and $CD4^+FoxP3^+$ cells harvested from GALT of GF controls and Hb-mono SW mice at 10 mpi

	GF	Hb
$B220^+$ ($\times 10^6$)		
Spleen	3.39 ± 0.51	4.25 ± 0.58
MLN	1.59 ± 0.39	1.99 ± 0.41
SI	0.11 ± 0.01	0.24 ± 0.05
Cecum	0.07 ± 0.01	0.43 ± 0.04[c]
Colon	0.16 ± 0.02	0.20 ± 0.02
$CD4^+IFN\gamma^+$ ($\times 10^3$)		
Spleen	151.9 ± 18.6	149.1 ± 22.8
MLN	58.9 ± 25.4	76.5 ± 23.9
SI	1.53 ± 0.21	2.38 ± 0.49[a]
Cecum	1.03 ± 0.17	6.87 ± 1.80[a]
Colon	1.88 ± 0.63	8.76 ± 3.77[a]
$CD4^+$ ($\times 10^6$)		
Spleen	2.23 ± 0.25	2.26 ± 0.19
MLN	1.57 ± 0.26	2.13 ± 0.27
SI	0.06 ± 0.01	0.09 ± 0.01[a]
Cecum	0.02 ± 0.01	0.10 ± 0.02[a]
Colon	0.01 ± 0.00	0.04 ± 0.01
$CD4^+FoxP3^+$ ($\times 10^3$)		
Spleen	590.5 ± 103	641.4 ± 61.3
MLN	340.9 ± 116	410.2 ± 81.9
SI	2.81 ± 0.89	11.47 ± 4.83[b]
Cecum	10.18 ± 3.08	21.86 ± 2.36[a]
Colon	8.68 ± 3.44	28.36 ± 4.78[a]
$CD4^+IL17^+$ ($\times 10^3$)		
Spleen	2.00 ± 0.38	0.94 ± 0.22
MLN	3.25 ± 1.38	3.25 ± 0.53
SI	2.23 ± 0.74	2.22 ± 0.37
Cecum	0.57 ± 0.18	5.63 ± 1.66[a]
Colon	0.96 ± 0.47	3.31 ± 1.78

GF, $n = 4$; Hb, $n = 7$.
[a]$P < 0.05$, [b]$P < 0.01$, [c]$P < 0.001$ regarding comparison of Hb-mono mice with control GF mice.

Scattered periportal vascular lesions of mononuclear cell accumulation suggested these lesions resulted from seeding the liver with Hb or associated antigens from the portal circulation. Although subclinical, the increased epithelial defects observed in older Hb-colonized mice could be associated with changes in intestinal barrier function and permit antigen showering of the liver.[2] Perivenular lymphoid aggregates were suggestive of TLT in the liver, as has previously been reported in male A/JCr mice infected with a novel EHS[37] later identified as *H. magdeburgensis*.[40] Immunohistochemistry for TLT did not confirm immune activation in these perivenular lymphoid aggregates, in contrast to the robust TLT demonstrated in GALT of the lower bowel. Other markers of TLT may prove useful in future studies of EHS-mediated liver lesions.

By repeating the 1-mpi evaluation with larger numbers of mice, we found that Hb stimulated increased numbers and the total area of lymphoid aggregates with large GC defined as those with apoptotic cells, tingible body macrophages, HEV, and ectatic lymphatics. Because tingible body macrophages are macrophages that have ingested apoptotic cells, their numbers should increase along with increased apoptosis. HEV increased in Hb-colonized mice may have been due to increased demand for tissue perfusion, consistent with GALT hyperplasia, or inflammation, consistent with mild enterocolitis. Additional evidence for GC activation included increased immunohistochemistry staining for apoptosis (cleaved caspase 3), antigen presentation (MHC class II), and MECA79 (MAdCAM), thus supporting increased trafficking of lymphocytes through the endothelium in TLT. Ectatic lymphatics were likewise evidence of increased lymphocyte traffic and were increased in Hb-colonized mice, supporting GC activation by Hb.

The regulatory milieu that developed in response to Hb had an antiinflammatory effect. In another study, the antiinflammatory activity of Hb was indicated by its amelioration of inflammatory sequela in the *H. pylori* gastritis model in C57BL/6 mice; in that case, Hb converted the anticipated *H. pylori*-associated Th1 cytokine responses into a more antiinflammatory Th2-like response.[24] However, Hb also stimulated *IL17* expression in our gnotobiotic model, consistent with reports that Hb promoted inflammatory lesions in an otherwise clinically silent, low-dose dodecyl sodium sulfate colitis model in immunocompetent mice[14] and in various colitis models in immune-dysregulated mice.[43] Proinflammatory effects of Hb and other EHS have been shown to be dependent on colonization with other microbiota in a colitis model using Hb-infected C3H/HeN mice[20] and in gnotobiotic $B6IL10^{-/-}$ mice that developed colitis only when *H. hepaticus* was cocolonized with *L. reuteri*.[45]

Hb stimulated enterocolitis that resulted in *CXCL13*-mediated $B220^+$ cell recruitment and, secondarily, *CCL21*-mediated T-cell chemotaxis to the cecum, with a similar trend in the colon. Other chemokines and cytokines induced by Hb promoted dendritic cell and stromal organization into TLT, resembling lymph node architecture. mRNA levels for *LT*β, which promotes GC formation, were significantly increased in response to Hb. In addition, Hb monoassociation upregulated *IFN*γ and *IL17* expression. Importantly, Hb induced a significant homeostatic response evident as elevated *IL10* mRNA expression and increased numbers of $CD4^+FoxP3^+$ regulatory cells. mRNA expression levels for *IL10*, which suppresses colitis in mouse models of inflammatory bowel disease,[33] were persistently upregulated in cecal tissue and colon at 1 and 10 mpi in Hb-mono mice.

Numbers of $CD4^+IL17^+$ in Hb-colonized mice and $CD4^+$ $IFN\gamma^+$ cells in the small intestine of Hb mice were not significantly increased; however, a statistical trend toward an increase was evident. Because Hb promoted differentiation of $CD4^+IL17^+$ cells, it could potentially be used to model IL17 pathophysiology. Some effects were tissue-dependent, with Hb colonizing in highest levels at the ileocecal–colic junction. Furthermore, the results indicate that the effects on GALT extended beyond the natural colonization niche of Hb. The increases in $CD4^+IL17^+$ subpopulations isolated from the MLN of Hb-colonized mice support the value of evaluating secondary lymphoid tissues that reflect lymphocyte trafficking.[15]

In summary, our findings suggest that Hb, which is considered a commensal in most immunocompetent mice, can be an opportunistic pathogen in select strains and stocks. The immunomodulatory effects suggest Hb should be considered a 'pathosymbiont provocateur'—that is, a member of the microbiome that can be clinically silent but has the potential to exacerbate or reduce inflammatory responses to gastrointestinal disease in mice and potentially humans. The current study suggests that GALT-associated TLT may be induction sites through which Hb suppresses inflammation via IL10 and regulatory T cells, consistent with a previous report on *H. hepaticus*.[47] Cocolonization of Hb with other microbiota may favor proinflammatory

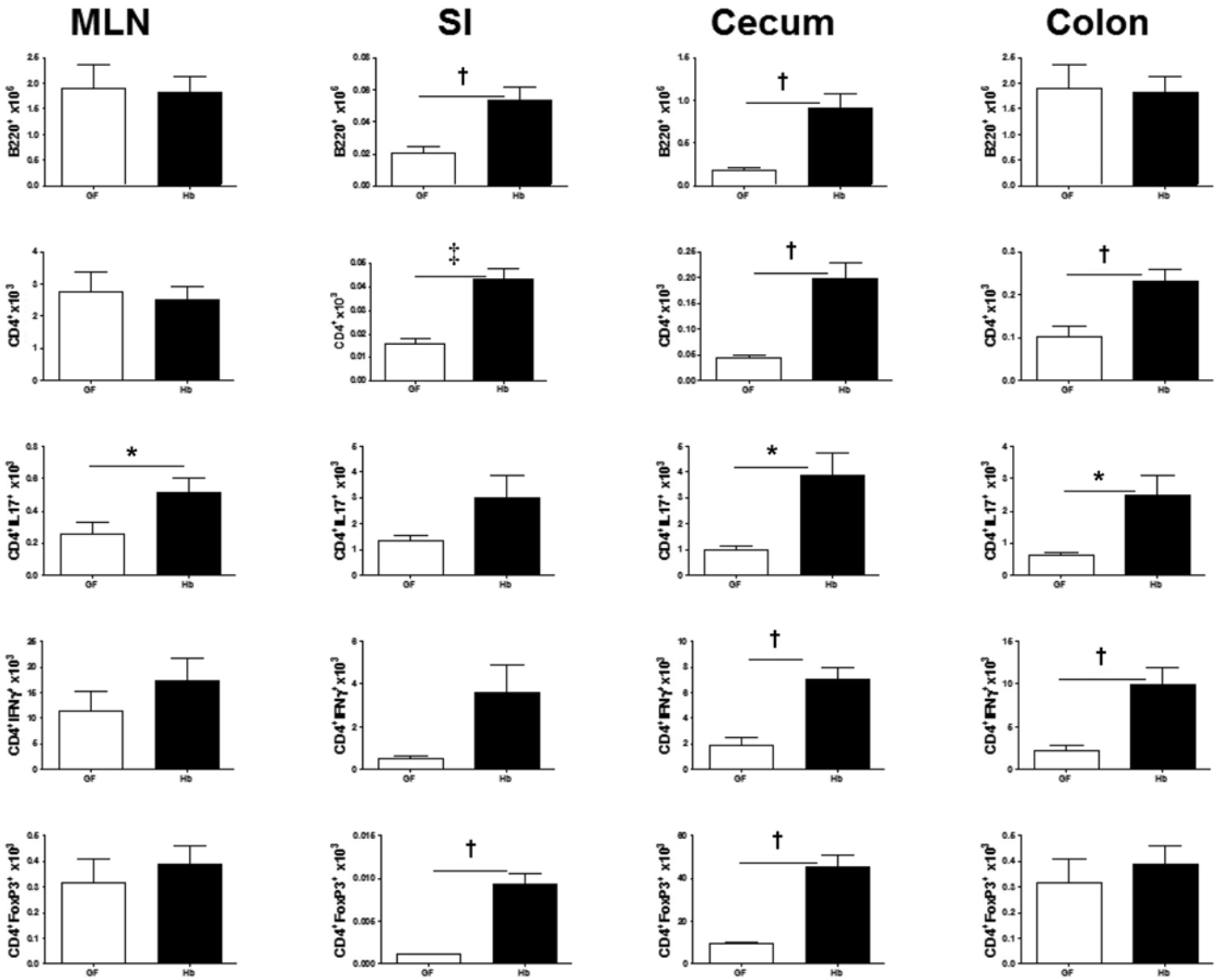

Figure 11. Absolute numbers (mean ± SE) for $B220^+$, $CD4^+$, $CD4^+IL17^+$, $CD4^+IFN\gamma^+$, and $CD4^+FoxP3^+$ cells in mesenteric lymph node (MLN) and lamina propria cells isolated from small intestine (SI), cecum, and colon of GF and Hb-mono mice at 1 mpi. n = 3–12 per group). *, $P < 0.05$; †, $P < 0.01$; ‡, $P < 0.001$.

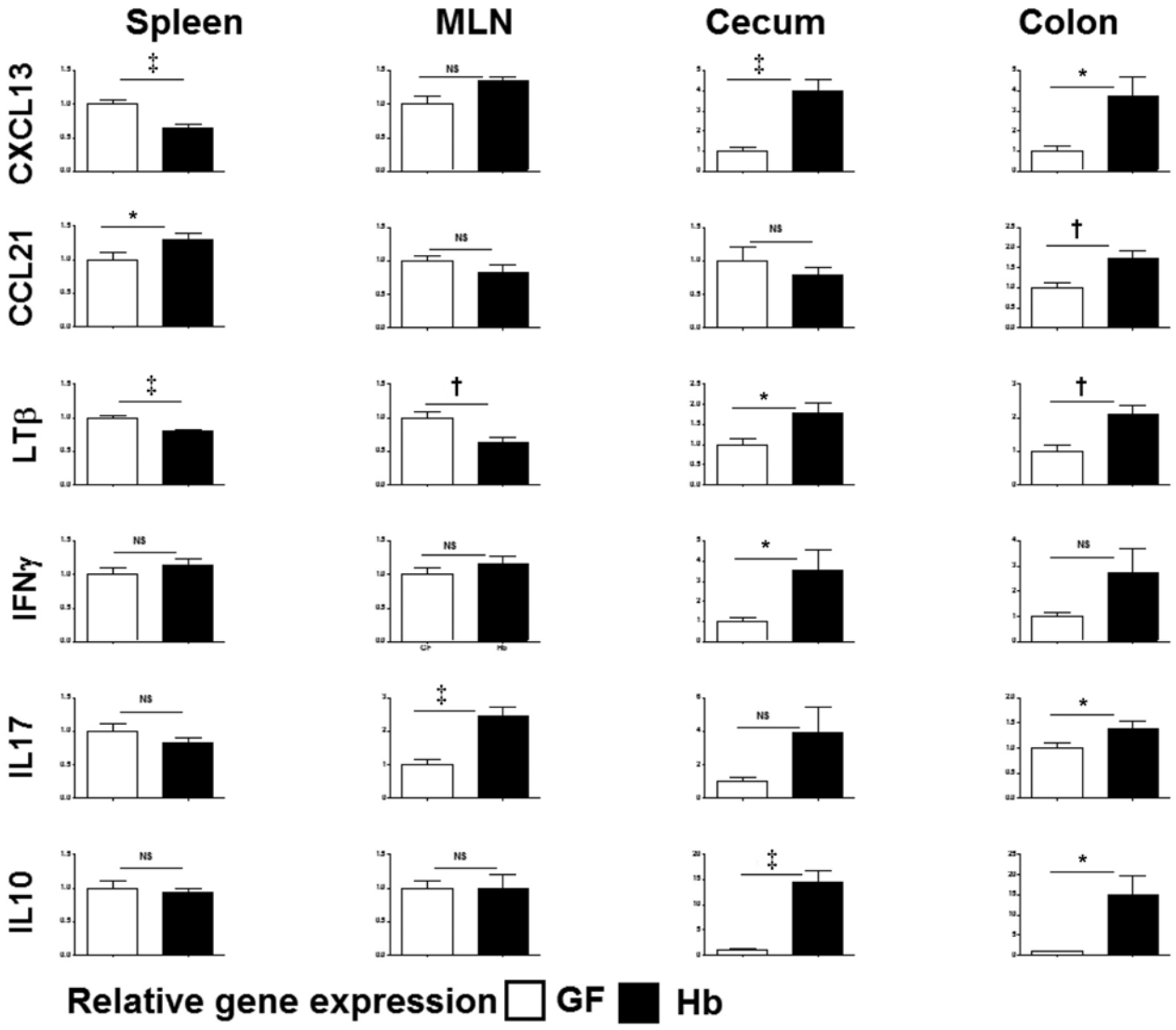

Figure 12. mRNA levels (mean ± 1 SD) of chemokines and cytokines at 1 mpi in spleen, mesenteric lymph node (MLN), cecum and colon in GF and gnotobiotic SW mice colonized with Hb (n = 8–12 per group). *, $P < 0.05$; †, $P < 0.01$; ‡, $P < 0.001$; NS, not significant.

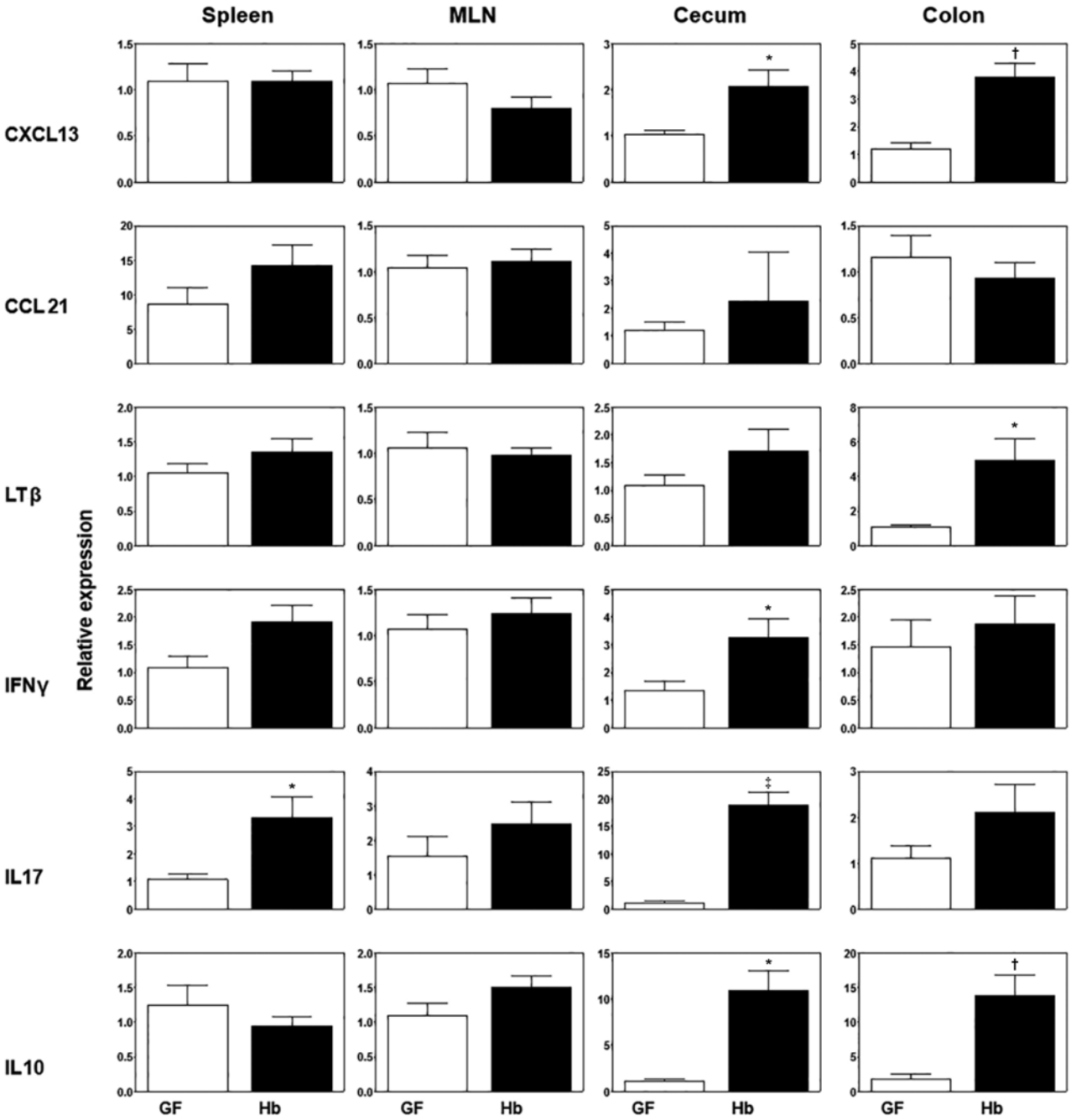

Figure 13. Cytokine and chemokine responses (mean ± SE) in GF and Hb-mono SW mice 10 mpi. n = 6–10 per group. *, $P < 0.05$; †, $P < 0.01$; ‡, $P < 0.001$.

responses in response to Hb infection, as we reported previously.[44] Continued study of Hb in gnotobiotic mice will potentially provide in-depth mechanistic data on Hb's effects on GALT development that can perhaps be applied to other mouse models of Hb-associated human disease.

Acknowledgments

This research was supported by the following grants to James G Fox: 1R01OD011141, P01 CA028842, P30–ES02109, and T32 OD010978. We extend special thanks to Carlos Umana, Allen Discua, Yassin Ibrahim, and Oscar Acevedo for their expert care of the gnotobiotic mice. We are very grateful to Christian Kaufman, Lenzie Cheney, and Dylan Puglisi for valuable assistance in necropsy and to Joanna Richards and Caroline Atkinson for histology preparations.

References

1. **Boivin GP, Washington K, Yang K, Ward JM, Pretlow TP, Russell R, Besselsen DG, Godfrey VL, Doetschman T, Dove WF, Pitot HC, Halberg RB, Itzkowitz SH, Groden J, Coffey RJ.** 2003. Pathology of mouse models of intestinal cancer: consensus report and recommendations. Gastroenterology **124:**762–777. https://doi.org/10.1053/gast.2003.50094.

2. **Brandl K, Kumar V, Eckmann L.** 2017. Gut-liver axis at the frontier of host-microbial interactions. Am J Physiol Gastrointest Liver Physiol **312:**G413–G419. https://doi.org/10.1152/ajpgi.00361.2016.
3. **Carter JW, Lancaster HK, Hardman WE, Cameron IL.** 1994. Distribution of intestine-associated lymphoid tissue, aberrant crypt foci, and tumors in the large bowel of 1,2-dimethylhydrazine-treated mice. Cancer Res **54:**4304–4307.
4. **Cesta MF.** 2006. Normal structure, function, and histology of mucosa-associated lymphoid tissue. Toxicol Pathol **34:**599–608. https://doi.org/10.1080/01926230600865531.
5. **Drazenovich NL, Franklin CL, Livingston RS, Besselsen DG.** 2002. Detection of rodent *Helicobacter* spp. by use of fluorogenic nuclease polymerase chain reaction assays. Comp Med **52:**347–353.
6. **Elmore SA.** 2006. Enhanced histopathology of mucosa-associated lymphoid tissue. Toxicol Pathol **34:**687–696. https://doi.org/10.1080/01926230600939989.
7. **Elmore SA.** 2010. Enhanced histopathology evaluation of lymphoid organs. Methods Mol Biol **598:**323–339. https://doi.org/10.1007/978-1-60761-401-2_22.
8. **Fox JG.** 2002. The non-*H pylori* helicobacters: their expanding role in gastrointestinal and systemic diseases. Gut **50:**273–283. https://doi.org/10.1136/gut.50.2.273.
9. **Fox JG, Dewhirst FE, Shen Z, Feng Y, Taylor NS, Paster BJ, Ericson RL, Lau CN, Correa P, Araya JC, Roa I.** 1998. Hepatic *Helicobacter* species identified in bile and gallbladder tissue from chileans with chronic cholecystitis. Gastroenterology **114:**755–763. https://doi.org/10.1016/S0016-5085(98)70589-X.
10. **Fox JG, Rogers AB, Whary MT, Taylor NS, Xu S, Feng Y, Keys S.** 2004. *Helicobacter bilis*-associated hepatitis in outbred mice. Comp Med **54:**571–577.
11. **Fox JG, Shen Z, Muthupalani S, Rogers AR, Kirchain SM, Dewhirst FE.** 2009. Chronic hepatitis, hepatic dysplasia, fibrosis, and biliary hyperplasia in hamsters naturally infected with a novel *Helicobacter* classified in the *H. bilis* cluster. J Clin Microbiol **47:**3673–3681. https://doi.org/10.1128/JCM.00879-09.
12. **Fox JG, Yan LL, Dewhirst FE, Paster BJ, Shames B, Murphy JC, Hayward A, Belcher JC, Mendes EN.** 1995. *Helicobacter bilis* sp. nov., a novel *Helicobacter* species isolated from bile, livers, and intestines of aged, inbred mice. J Clin Microbiol **33:**445–454. https://doi.org/10.1128/JCM.33.2.445-454.1995.
13. **Franklin CL, Riley LK, Livingston RS, Beckwith CS, Besch-Williford CL, Hook RR Jr.** 1998. Enterohepatic lesions in SCID mice infected with *Helicobacter bilis*. Lab Anim Sci **48:**334–339.
14. **Gomes-Neto JC, Kittana H, Mantz S, Segura Munoz RR, Schmaltz RJ, Bindels LB, Clarke J, Hostetter JM, Benson AK, Walter J, Ramer-Tait AE.** 2017. A gut pathobiont synergizes with the microbiota to instigate inflammatory disease marked by immunoreactivity against other symbionts but not itself. Sci Rep **7:**1–14. https://doi.org/10.1038/s41598-017-18014-5.
15. **Habtezion A, Nguyen LP, Hadeiba H, Butcher EC.** 2016. Leukocyte trafficking to the small intestine and colon. Gastroenterology **150:**340–354. https://doi.org/10.1053/j.gastro.2015.10.046.
16. **Haines DC, Gorelick PL, Battles JK, Pike KM, Anderson RJ, Fox JG, Taylor NS, Shen Z, Dewhirst FE, Anver MR, Ward JM.** 1998. Inflammatory large bowel disease in immunodeficient rats naturally and experimentally infected with *Helicobacter bilis*. Vet Pathol **35:**202–208. https://doi.org/10.1177/030098589803500305.
17. **Hänninen ML, Kärenlampi RI, Koort JM, Mikkonen T, Björkroth KJ.** 2005. Extension of the species *Helicobacter bilis* to include the reference strains of *Helicobacter* sp. flexispira taxa 2, 3 and 8 and Finnish canine and feline flexispira strains. Int J Syst Evol Microbiol **55:**891–898. https://doi.org/10.1099/ijs.0.63245-0.
18. **Hansen R, Thomson JM, Fox JG, El-Omar EM, Hold GL.** 2010. Could *Helicobacter* organisms cause inflammatory bowel disease? FEMS Immunol Med Microbiol **61:**1–14. https://doi.org/10.1111/j.1574-695X.2010.00744.x.
19. **Institute for Laboratory Animal Research.** 2011. Guide for the care and use of laboratory animals, 8th ed. Washington (DC): National Academies Press.
20. **Jergens AE, Wilson-Welder JH, Dorn A, Henderson A, Liu Z, Evans RB, Hostetter J, Wannemuehler MJ.** 2007. *Helicobacter bilis* triggers persistent immune reactivity to antigens derived from the commensal bacteria in gnotobiotic C3H/HeN mice. Gut **56:**934–940. https://doi.org/10.1136/gut.2006.099242.
21. **Kanamori Y, Ishimaru K, Nanno M, Maki K, Ikuta K, Nariuchi H, Ishikawa H.** 1996. Identification of novel lymphoid tissues in murine intestinal mucosa where clusters of c-kit+ IL-7R+ Thy1+ lympho-hemopoietic progenitors develop. J Exp Med **184:**1449–1459. https://doi.org/10.1084/jem.184.4.1449.
22. **Kuper CF.** 2006. Histopathology of mucosa-associated lymphoid tissue. Toxicol Pathol **34:**609–615. https://doi.org/10.1080/01926230600867735.
23. **Kuper CF, Harleman JH, Richter-Reichelm HB, Vos JG.** 2000. Histopathologic approaches to detect changes indicative of immunotoxicity. Toxicol Pathol **28:**454–466. https://doi.org/10.1177/019262330002800317.
24. **Lemke LB, Ge Z, Whary MT, Feng Y, Rogers AB, Muthupalani S, Fox JG.** 2009. Concurrent *Helicobacter bilis* infection in C57BL/6 mice attenuates proinflammatory *H. pylori*-induced gastric pathology. Infect Immun **77:**2147–2158. https://doi.org/10.1128/IAI.01395-08.
25. **Lofgren JL, Esmail M, Mobley M, McCabe A, Taylor NS, Shen Z, Erdman S, Hewes C, Whary MT, Fox JG.** 2012. Prevalence of murine *Helicobacter* spp. Infection is reduced by restocking research colonies with *Helicobacter*-free mice. J Am Assoc Lab Anim Sci **51:**436–442.
26. **Maggio-Price L, Bielefeldt-Ohmann H, Treuting P, Iritani BM, Zeng W, Nicks A, Tsang M, Shows D, Morrissey P, Viney JL.** 2005. Dual infection with *Helicobacter bilis* and *Helicobacter hepaticus* in p-glycoprotein-deficient *mdr1a*$^{-/-}$ mice results in colitis that progresses to dysplasia. Am J Pathol **166:**1793–1806. https://doi.org/10.1016/S0002-9440(10)62489-3.
27. **Maggio-Price L, Shows D, Waggie K, Burich A, Zeng W, Escobar S, Morrissey P, Viney JL.** 2002. *Helicobacter bilis* infection accelerates and *H. hepaticus* infection delays the development of colitis in multiple drug resistance-deficient (*mdr1a*$^{-/-}$) mice. Am J Pathol **160:**739–751. https://doi.org/10.1016/S0002-9440(10)64894-8.
28. **Matsukura N, Yokomuro S, Yamada S, Tajiri T, Sundo T, Hadama T, Kamiya S, Naito Z, Fox JG.** 2002. Association between *Helicobacter bilis* in bile and biliary tract malignancies: *H. bilis* in bile from Japanese and Thai patients with benign and malignant diseases in the biliary tract. Jpn J Cancer Res **93:**842–847. https://doi.org/10.1111/j.1349-7006.2002.tb01327.x.
29. **Moser CA, Dolfi DV, Di Vietro ML, Heaton PA, Offit PA, Clark HF.** 2001. Hypertrophy, hyperplasia, and infectious virus in gut-associated lymphoid tissue of mice after oral inoculation with simian-human or bovine-human reassortant rotaviruses. J Infect Dis **183:**1108–1111. https://doi.org/10.1086/319294.
30. **Murata H, Tsuji S, Tsujii M, Fu HY, Tanimura H, Tsujimoto M, Matsuura N, Kawano S, Hori M.** 2004. *Helicobacter bilis* infection in biliary tract cancer. Aliment Pharmacol Ther **20 Suppl 1:**90–94. https://doi.org/10.1111/j.1365-2036.2004.01972.x.
31. **Nguyen DD, Muthupalani S, Goettel JA, Eston MA, Mobley M, Taylor NS, McCabe A, Marin R, Snapper SB, Fox JG.** 2013. Colitis and colon cancer in WASP-deficient mice require *Helicobacter spp*. Inflamm Bowel Dis **19:**2041–2050. https://doi.org/10.1097/MIB.0b013e318295fd8f.
32. **Pisani P, Whary MT, Nilsson I, Sriamporn S, Wadstrom T, Fox JG, Ljungh A, Forman D.** 2008. Cross-reactivity between immune responses to *Helicobacter bilis* and *Helicobacter pylori* in a population in Thailand at high risk of developing cholangiocarcinoma. Clin Vaccine Immunol **15:**1363–1368. https://doi.org/10.1128/CVI.00132-08.
33. **Redhu N, Shouval D, Bakthavatchalu V, Wang C, Conaway E, Goettel J, Mack M, Bleich A, Bry L, Fox J, Snapper S, Horwitz B.** 2016. O-005 YI microbiota drives inflammation by altering intestinal lamina propria macrophage phenotype in a novel IL10R-deficient model of very early onset IBD. Inflamm Bowel Dis **22 Suppl 1:**S2–S3. https://doi.org/10.1097/01.MIB.0000480043.65761.b2.
34. **Rogers AB, Cormier KS, Fox JG.** 2006. Thiol-reactive compounds prevent nonspecific antibody binding in immunohistochemistry. Lab Invest **86:**526–533. https://doi.org/10.1038/labinvest.3700407.
35. **Segura-López FK, Avilés-Jiménez F, Güitrón-Cantú A, Valdéz-Salazar HA, León-Carballo S, Guerrero-Pérez L, Fox JG, Torres J.**

2015. Infection with *Helicobacter bilis* but not *Helicobacter hepaticus* was associated with extrahepatic cholangiocarcinoma. Helicobacter **20:**223–230. https://doi.org/10.1111/hel.12195.

36. **Shomer NH, Dangler CA, Schrenzel MD, Fox JG.** 1997. *Helicobacter bilis*-induced inflammatory bowel disease in *scid* mice with defined flora. Infect Immun **65:**4858–4864. https://doi.org/10.1128/IAI.65.11.4858-4864.1997.
37. **Shomer NH, Fox JG, Juedes AE, Ruddle NH.** 2003. *Helicobacter*-induced chronic active lymphoid aggregates have characteristics of tertiary lymphoid tissue. Infect Immun **71:**3572–3577. https://doi.org/10.1128/IAI.71.6.3572-3577.2003.
38. **Takahashi S, Tomita J, Nishioka K, Hisada T, Nishijima M.** 2014. Development of a prokaryotic universal primer for simultaneous analysis of bacteria and archaea using next-generation sequencing. PLoS One **9:**1–9. https://doi.org/10.1371/journal.pone.0105592.
39. **Taylor NS, Xu S, Nambiar P, Dewhirst FE, Fox JG.** 2007. Enterohepatic *Helicobacter* species are prevalent in mice from commercial and academic institutions in Asia, Europe, and North America. J Clin Microbiol **45:**2166–2172. https://doi.org/10.1128/JCM.00137-07.
40. **Traverso FR, Bohr UR, Oyarzabal OA, Rohde M, Clarici A, Wex T, Kuester D, Malfertheiner P, Fox JG, Backert S.** 2010. Morphologic, genetic, and biochemical characterization of *Helicobacter magdeburgensis*, a novel species isolated from the intestine of laboratory mice. Helicobacter **15:**403–415. https://doi.org/10.1111/j.1523-5378.2010.00770.x.
41. **Wang C, Thangamani S, Kim M, Gu BH, Lee JH, Taparowsky EJ, Kim CH.** 2013. BATF is required for normal expression of gut-homing receptors by T helper cells in response to retinoic acid. J Exp Med **210:**475–489. https://doi.org/10.1084/jem.20121088.
42. **Ward JM, Fox JG, Anver MR, Haines DC, George CV, Collins MJ Jr, Gorelick PL, Nagashima K, Gonda MA, Gilden RV, Tully JG, Russell RJ, Benvensite RE, Paster BJ, Dewhirst FE, Donovan JC, Anderson LM, Rice JM.** 1994. Chronic active hepatitis and associated liver tumors in mice caused by a persistent bacterial infection with a novel *Helicobacter species*. J Natl Cancer Inst **86:**1222–1227. https://doi.org/10.1093/jnci/86.16.1222.
43. **Whary MT, Fox JG.** 2004. Natural and experimental *Helicobacter* infections. Comp Med **54:**128–158.
44. **Whary MT, Fox JG.** 2006. Detection, eradication, and research implications of *Helicobacter* infections in laboratory rodents. Lab Anim (NY) **35:**25–27, 30–36. https://doi.org/10.1038/laban0706-25.
45. **Whary MT, Taylor NS, Feng Y, Ge Z, Muthupalani S, Versalovic J, Fox JG.** 2011. *Lactobacillus reuteri* promotes *Helicobacter hepaticus*-associated typhlocolitis in gnotobiotic B6.129P2-IL10^{tm1Cgn} (IL10$^{-/-}$) mice. Immunology **133:**165–178. https://doi.org/10.1111/j.1365-2567.2011.03423.x.
46. **Woods SE, Ek C, Shen Z, Feng Y, Ge Z, Muthupalani S, Whary MT, Fox JG.** 2015. Male Syrian hamsters experimentally infected with *Helicobacter* spp. of the *H. bilis* cluster develop MALT-associated gastrointestinal lymphomas. Helicobacter **21:**201–217. https://doi.org/10.1111/hel.12265.
47. **Xu M, Pokrovskii M, Ding Y, Yi R, Au C, Harrison OJ, Galan C, Belkaid Y, Bonneau R, Littman DR.** 2018. c-MAF-dependent regulatory T cells mediate immunological tolerance to a gut pathobiont. Nature **554:**373–377. https://doi.org/10.1038/nature25500.